

Early-age shrinkage effects in precast concrete sandwich panels

Qian Huang, Ehab Hamed, and R. Ian Gilbert

- Five precast concrete sandwich panels with different structural configurations were tested under ambient laboratory conditions to determine the panels' shrinkage strain behavior.
- The results of the experimental testing were used to develop strain profiles for finite element analysis to investigate the effect of key parameters on the early-age behavior of the precast concrete sandwich panels.
- The results of the study show that using a bilinear shrinkage profile for each concrete layer in the analysis accurately predicts the shrinkage strains and that early-age cracking can occur in precast concrete sandwich panels that are not properly cured or that have a high reinforcement ratio.

Precast concrete sandwich panels (PCSPs) are becoming popular because of their advantages in terms of rapid speed of construction, superior energy conservation, and flexible and diverse aesthetic options.^{1,2} PCSPs are widely used as structural members in residential buildings, hospitals, industrial warehouses, and schools.³ Traditional noncomposite PCSPs are commonly used and usually comprise one thick reinforced concrete layer and one thin layer of concrete cladding connected using mechanical anchors. Composite PCSPs that use shear connectors in the form of diagonal steel or fiber reinforced polymer (FRP) reinforcing bars to connect the two reinforced concrete layers are becoming popular due to their improved shear transfer mechanism and material savings.⁴ In composite PCSP applications, the two reinforced concrete layers are the same thickness, and the overall thickness of the panel is about $\frac{1}{2}$ to $\frac{2}{3}$ of a comparable noncomposite panel while still offering relatively similar structural and thermal insulation properties.³ No official standards have been established to date for designing PCSPs, and relatively little research has been reported on their early-age structural behavior.⁵ Because PCSPs are normally designed to ensure crack-free performance, a careful look at all potential causes of cracking is needed, especially at the panels' early age, while concrete is still immature with relatively low tensile strength.

The most critical aspects of structural behavior of concrete at an early age are thermal deformation and shrinkage. Thermal deformation is mainly caused by heat dissipation (cooling) of concrete after casting, when the hydration

PCI Journal (ISSN 0887-9672) V. 65, No. 1, January–February 2020.

PCI Journal is published bimonthly by the Precast/Prestressed Concrete Institute, 200 W. Adams St., Suite 2100, Chicago, IL 60606.

Copyright © 2020, Precast/Prestressed Concrete Institute. The Precast/Prestressed Concrete Institute is not responsible for statements made by authors of papers in *PCI Journal*. Original manuscripts and discussion on published papers are accepted on review in accordance with the Precast/Prestressed Concrete Institute's peer-review process. No payment is offered.

process takes place. The thermal contraction of concrete after hydration is more significant in large elements where the temperature gradient is very high, such as in dams, bridges, and power plants, whereas it is usually not an important problem in thin slabs or wall panels. Shrinkage, which is a time-dependent phenomenon, also leads to a reduction in the concrete volume. It is mainly caused by the combination of loss of moisture content (drying shrinkage) and continuous chemical reactions within concrete ingredients (autogenous shrinkage). Shrinkage strain varies through the depth of a concrete member because of temperature differences between the two faces of the member and the different degree of hydration through the depth. In reinforced concrete members, the steel reinforcement and connections to other members restrain shrinkage and thereby reduce the contraction of the member. As a result, these restraining forces induce internal tensile stresses and lead to elastic and creep deformations. This can lead to cracking, especially at an early age of concrete, which may not only cause serviceability and durability problems but may also reduce the aesthetic value.⁶⁻⁸

In PCSPs, the steel reinforcement, shear connectors, and bonding to the insulation layer provide significantly more restraint to the free shrinkage of concrete than is typical of the restraint in other reinforced concrete members, and this makes predicting the shrinkage strain profile a difficult task. The problem becomes worse if the panels are not adequately cured, leading to excessive moisture loss.^{4,5,9-11} Hence, shrinkage in PCSPs may cause severe premature cracking and curvature (bowing) at early ages. These effects will mostly take place while the panels are still at the warehouse of the precast concrete manufacturer prior to their distribution or on-site before installation. Once installed to the building, the preexisting tensile stresses in the concrete due to shrinkage will reduce the flexural cracking moment of the panel under lateral loads such as wind.

There has been no research undertaken to date on the shrinkage effects in PCSPs. Nevertheless, some of the literature that is related to shrinkage in concrete structures, which is useful for this study, is provided in the following paragraphs.

Pigeon et al.¹² tested the behavior of concrete prisms clamped at both ends at early ages. It was found that the viscoelasticity of concrete leads to relaxation of the tensile stresses caused by restrained shrinkage, which reduces cracking. The importance of the tensile creep and relaxation associated with shrinkage in restrained concrete was also highlighted by Weiss et al.,¹³ Kovler,¹⁴ Sule and van Breugel,¹⁵ and Altoubat and Lange.¹⁶ Khan et al.¹⁷ studied the early-age physical properties of concrete. Autogenous shrinkage in concrete was found to be more critical during the first two to three days after casting, while drying shrinkage became dominant afterwards.

Gilbert¹⁸ proposed a simplified method for estimating cracking due to restrained early-age deformation of concrete. However, the differential shrinkage through the thickness of the member was not discussed, and the model developed

cannot be easily applied to PCSPs due to their partially composite action. Gilbert et al.¹⁹ studied the effects of shrinkage in composite concrete slabs made with steel decks. It was found that the differential shrinkage distribution caused by the steel decking can lead to significant cracking. Similar results were reported in Gholamhoseini et al.²⁰ Al-deen and Ranzi²¹ also studied the nonuniform shrinkage effects in composite steel-concrete slabs. The authors indicated that assuming a uniform distribution of shrinkage strains through the thickness of the member may underestimate the deflections.

Kim and Lee²² developed an analytical model for the prediction of differential drying shrinkage in concrete. The model was based on the moisture diffusion approach proposed by Bažant and Najjar.²³ The shrinkage strains were assumed to be linearly proportional to the interior humidity in concrete members based on Bažant and Thonguthai,²⁴ Illston and Tajirian,²⁵ and Sakata.²⁶ The modeling approach also considered the effect of creep of concrete with the use of the simplified age-adjusted effective modulus. However, the method developed in Kim and Lee²² may not be easily applied to PCSPs due to their layered structural configuration.

In this study, shrinkage effects are examined in five PCSPs under ambient laboratory conditions. The study focuses on these effects at the early ages of concrete, such as during the first few weeks after termination of curing. A finite element analysis (FEA) model is also developed and validated to predict the PCSP behavior, which provides a useful tool for conducting parametric studies and to further explain the experimental findings and the structural response of the panels.

Experimental study

Shrinkage in PCSPs is restrained by the internal steel reinforcement, bonding to the insulation and the composite action provided by shear connectors. To clarify the role of each of these effects, the experimental program included a number of tests with various panel configurations. **Table 1** summarizes the details of the tested panels and their layouts, and cross sections are shown in **Figures 1** and **2**, respectively. Four of the five panels were 2700 mm (106 in.) long and 600 mm (24 in.) wide with two 50 mm (2 in.) thick reinforced concrete layers separated by a 50 mm thick layer of insulation. Panel 5 was similar, except that the reinforced concrete layers and the insulation layer were each 80 mm (3.1 in.) thick. The experimental study included the measurement of the shrinkage-induced strains for a period of 21 days. Shrinkage prisms of 75 × 75 × 280 mm (3 × 3 × 11 in.) were prepared (**Fig. 3**) to measure the free shrinkage of concrete.

Panel 1 was designed with no shear connectors and with plastic sheets between the concrete layers and the insulation. The testing procedure for panel 1 was chosen to isolate the effect of free shrinkage of concrete and the effect of restraint caused by the steel reinforcement used for reinforcing the wythes. The bottom concrete layer of panel 1 was reinforced with a steel mesh of 6 mm (0.24 in.) diameter round rein-

Table 1. Configurations of precast concrete sandwich panels

Specimen designation	Insulation	Thickness of concrete layer, mm	Reinforcement	GFRP connector size, mm
1	EPS	50	6 mm diameter at 200 mm spacing*	n/a
2	EPS	50	6 mm diameter at 200 mm spacing	n/a
3	XPS	50	6 mm diameter at 200 mm spacing	n/a
4	EPS	50	6 mm diameter at 200 mm spacing	6
5	EPS	80	8 mm diameter at 200 mm spacing	10

Note: EPS = expanded polystyrene; GFRP = glass-fiber-reinforced polymer; n/a = not applicable; XPS = extruded polystyrene. 1 mm = 0.03937 in.

* Reinforcement is provided only in bottom wythe.

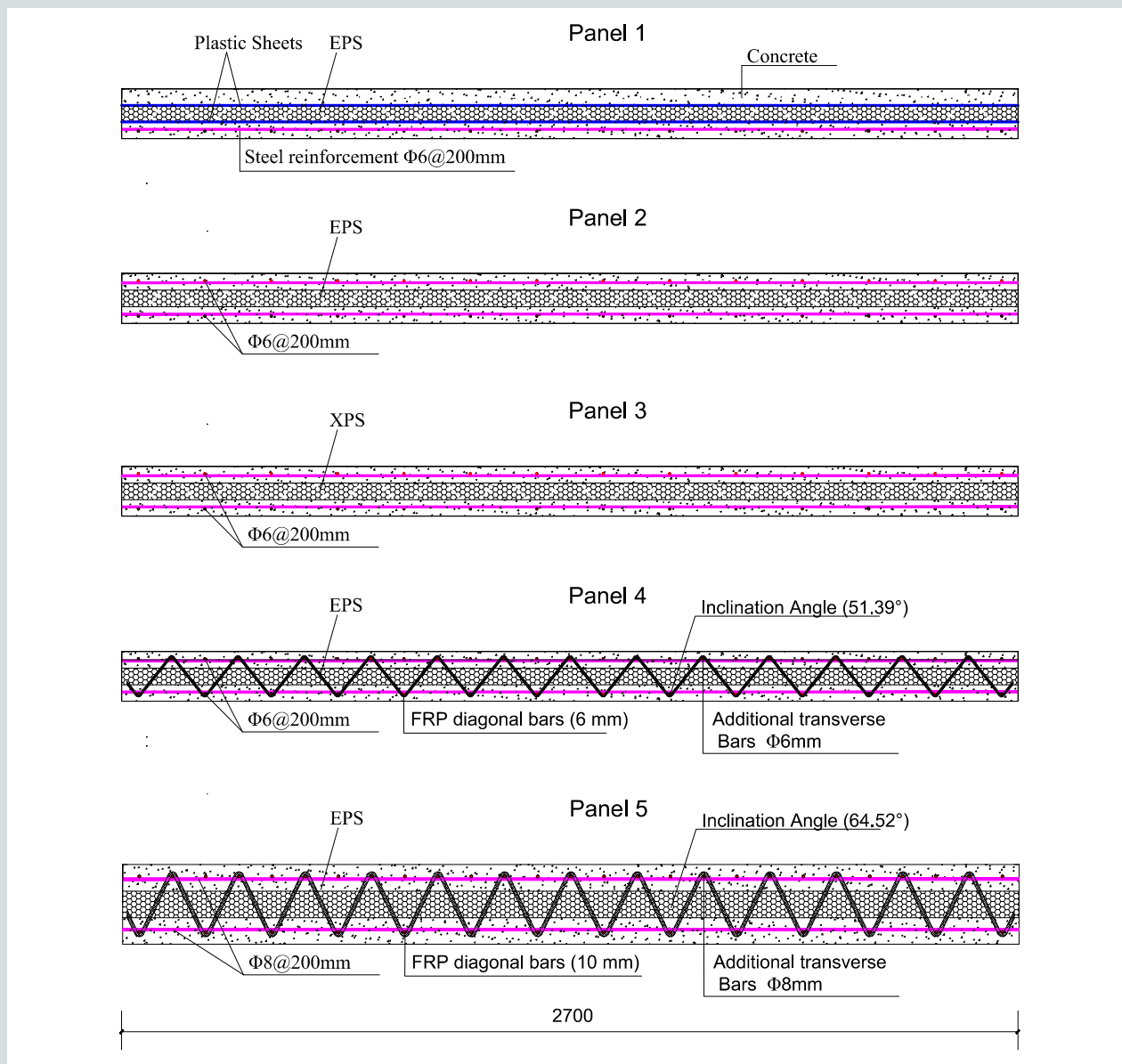


Figure 1. Longitudinal configuration of the precast concrete sandwich panels. Note: Dimensions are in millimeters. EPS = expanded polystyrene; FRP = fiber-reinforced polymer; XPS = extruded polystyrene. 1 mm = 0.03937 in. $\Phi 6$ = 6 mm diameter; $\Phi 8$ = 8 mm diameter

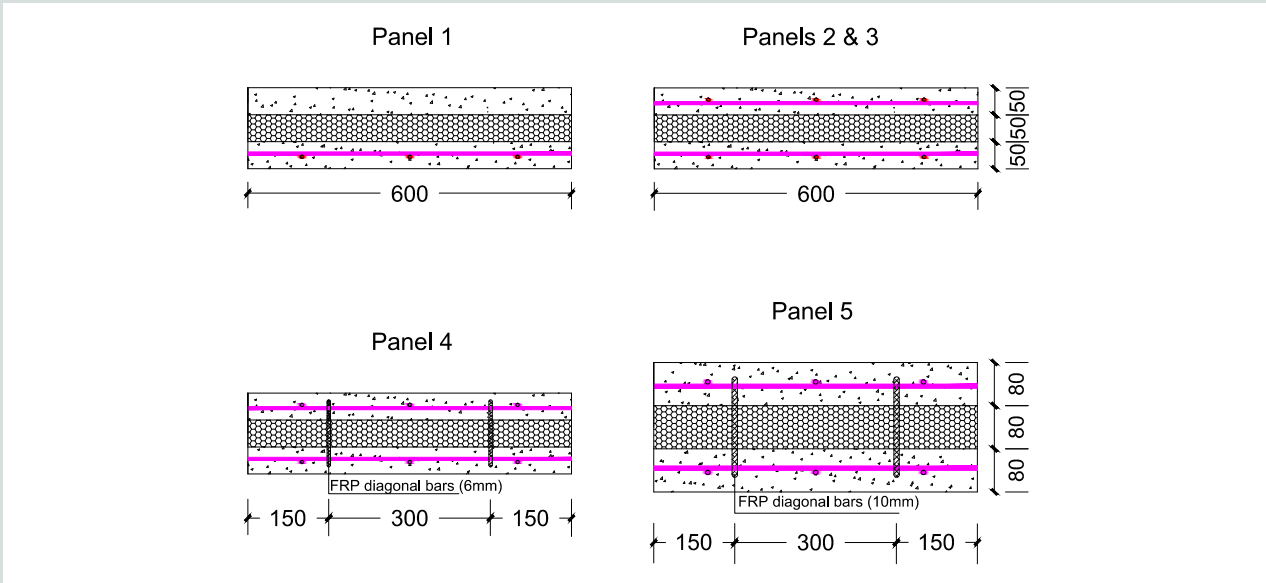


Figure 2. Cross sections of the precast concrete sandwich panels. Note: Dimensions are in millimeters. FRP = fiber-reinforced polymer. 1 mm = 0.03937 in.



Figure 3. Shrinkage tests.

forcing bars at a spacing of 200 mm (8 in.). The top concrete layer of panel 1 remained unreinforced to approximately evaluate free shrinkage, assuming that friction is negligible. This type of panel does not exist in practice but is used here to serve the purpose of this investigation. It is expected that free shrinkage strains in a layered structural configuration will be different from those measured in a prism that is exposed on all sides to the environment. The effect of a layered configuration on shrinkage strains will be clarified through the results obtained from the top unrestrained layer of panel

1 because its top surface is fully exposed to the environment, with accelerated drying of concrete, whereas the bottom surface is not exposed.

Panel 2 was also designed with no shear connectors with the goal of isolating the effect of restraint on shrinkage strains caused by the bonding between the concrete and the insulation layer. The panel was constructed with two reinforced concrete layers that were bonded to an expanded polystyrene (EPS) insulation layer. Panel 3 was similar to panel 2, but it

was constructed with extruded polystyrene (XPS) insulation. The comparison of panels 2 and 3 was used to study the differences between the shrinkage restraint provided by EPS and XPS insulation.

Panel 4 was similar to panel 2, but it included continuous glass FRP (GFRP) diagonal-bar shear connectors of 6 mm (0.24 in.) diameter. The layout of this panel is shown in Figure 1, and its cross section is shown in Figure 2. The results from panel 4 compared with the results from panel 2 can clarify the effect of the restraint caused by the shear connectors. Finally, for investigating the effect of layer thickness on shrinkage, panel 5 was made with thicker layers but with almost the same reinforcement ratio as panel 4. Larger-diameter FRP bars were used in panel 5 (Fig. 2).

All panels were cast using a commercially mixed concrete made with 10 mm (0.4 in.) aggregate and a 260 mm (10.2 in.) slump. After casting, the panels were covered with wet burlap and plastic sheets. Moist curing was provided for seven days before stripping. After curing, all specimens were supported at three locations: both edges and midlength (Fig. 3). The shrinkage-induced strains were then measured under ambient laboratory conditions for 21 days until the age of concrete reached 28 days. The average temperature and humidity in the laboratory were 23.5°C (74.3°F) and 54%, respectively, with relatively small fluctuations during the testing period. For each panel, the strains were measured at three points through the thickness of the top concrete layer at a distance of 675 mm (26.6 in.) from both edges. Vibrating-wire strain gauges were embedded at the interface of the bottom of the top concrete layer and the insulation and at midthickness of the top concrete layer. A polyester wire strain gauge was used to measure the strain on the top surface of the panels. For panel 1, the strains in the bottom reinforced concrete layer were also measured at the same locations through the thickness—that is,

bottom panel surface, midthickness of the bottom layer, and interface of the top of the bottom layer and the insulation. All specimens were loaded to failure under four-point bending after the shrinkage measurements. Their failure loading and behavior will be reported in a future study.

Finite element analysis

The FEA used a two-dimensional modeling approach to simulate the behavior of PCSPs in Abaqus, which is a commercially available FEA software package. The concrete-to-insulation interfaces were assumed to be fully bonded for panels 2 to 5. For panel 1, where plastic sheets were installed, no bonding or friction was introduced at the interfaces, allowing only for contact. The continuous diagonal-bar shear connectors were rigidly connected to the steel mesh reinforcement and were assumed fully bonded to the concrete and the insulation core. The steel reinforcement was also assumed fully bonded to the concrete. Four node plane strain elements (CPE4) with two degrees of freedom at each node were used to model the concrete layers and the insulation. The steel mesh reinforcement and the diagonal reinforcing bars used two-node one-dimensional truss elements. Approximately 10 elements were generated through the thickness of the concrete and insulation layers and along the diagonal bars. Tie constraints were automatically generated across interfaces with incompatible meshes.

The two-dimensional modeling approach has been previously validated by the authors using a comparison to experimental results from the literature and a comparison to a three-dimensional model.²⁷ Figure 4 shows the FEA model. Shrinkage strain was simulated as a thermal strain in the FEA model because the models are similar for the two problems. Temperature was induced in the structure, but the coefficient of thermal expansion of the steel reinforcement, the FRP, and the

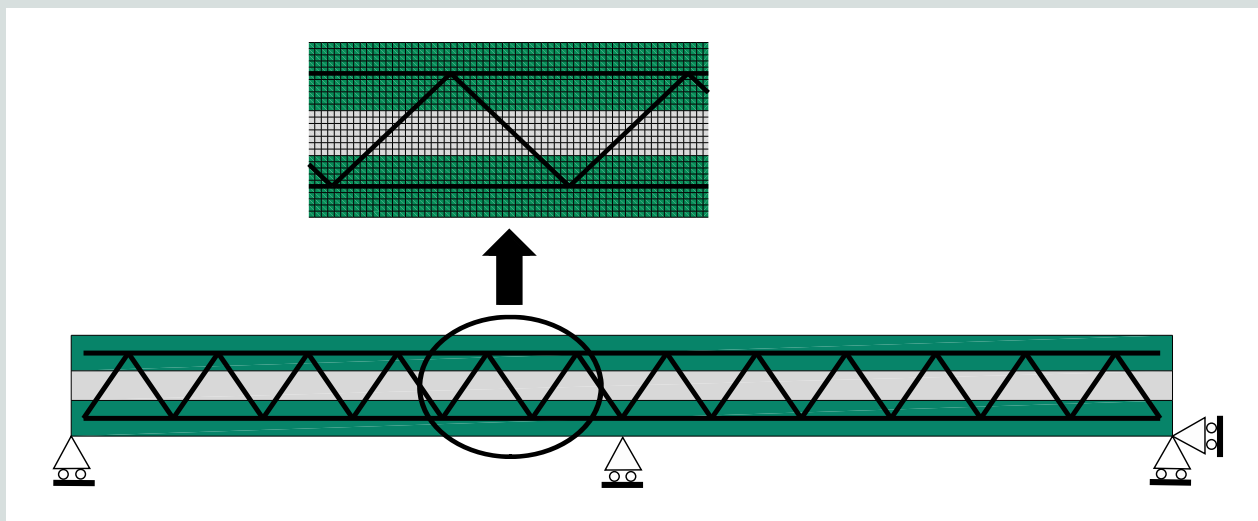


Figure 4. Finite element model and meshing.

insulation were set to zero to simulate shrinkage of concrete only. The temperature level was chosen to induce a thermal strain in the concrete that was equal to the shrinkage strain.

The constitutive relations of the concrete account for the effects of creep, shrinkage, and aging. Because the goal of this study was to check the possibility of early cracking of concrete under restrained shrinkage, the concrete was assumed linear viscoelastic in both compression and tension at the precracking stage. Once the stress exceeds the tensile strength, cracks are assumed to develop and the analysis will stop. To conduct a time-stepping analysis due to the variation of stresses and strains with time, a rheological model that was applied by Bažant and Wu²⁸ for the creep analysis of concrete was adopted in the FEA model. The model is based on the generalized Maxwell chain and can be implemented in Abaqus. Assuming the same creep characteristics in both tension and compression, the relaxation modulus of concrete $R(t, t')$ is assumed to be equal to the effective modulus as follows:

$$R(t, t') = \frac{E_c(t)}{1 + \phi(t, t')}$$

where

$E_c(t)$ = time-dependent elastic modulus of concrete that is increasing due to aging

$\phi(t, t')$ = creep coefficient of concrete at time t for a load applied at time t'

To implement the generalized Maxwell chain model, the relaxation modulus is expanded into a Dirichlet series, and the approximated relaxation modulus $R'(t, t')$ is expressed as

$$R'(t, t') = \sum_{\mu=1}^n E_{\mu}(t') e^{-(t-t')/\tau_{\mu}} + E_{n+1}(t')$$

where

n = number of spring-dashpot units

μ = unit number

$E_{\mu}(t')$ = modulus of the μ th spring in the Maxwell chain for a strain applied at time t'

τ_{μ} = relaxation time of the μ th unit

Five Maxwell units are used to model the viscoelastic response of concrete.

In this study, the creep coefficient $\phi(t, t')$ of concrete follows ACI's *Prediction of Creep, Shrinkage, and Temperature Effects in Concrete Structures*:²⁹

$$\phi(t, t') = \frac{(t-t')^w}{d + (t-t')^w} \phi_u$$

where

d = constant taken as 10 for standard conditions

ψ = constant taken as 0.6 for standard conditions

ϕ_u = final creep coefficient that depends on the age of first loading and is taken as $2.35\gamma_c$, where γ_c is the cumulative product of correction factors

For this FEA model, the creep coefficient was determined at the concrete age of seven days.

Carol and Bažant³⁰ showed that the solidification model developed in Bažant and Prasannan³¹ for handling the aging and creep phenomena is equivalent to the well-known rheological Maxwell or Kelvin models but with spring constants that increase proportionally to the same function $\zeta(t)$. The function $\zeta(t)$ is referred to as the aging function; it describes the increase in the macroscopic elastic modulus over time and guarantees continuously increasing positive values for the spring constants. Because of the continuous change in the stress and strain distributions due to shrinkage over time, the spring modulus in the generalized Maxwell chain can be expressed as $E_{\mu}(t) = E_{\mu}(t) = \zeta(t)E_{\mu}$, where E_{μ} is determined only once (at the age of initial loading) using the least squares approach. The aging function is determined as the ratio between the time-dependent elastic modulus and its magnitude at the time of initial loading t_0 .

$$\zeta(t) = \frac{E_c(t)}{E_c(t_0)}$$

The time-dependent elastic modulus is determined from

$$E_c(t) = \sqrt{\frac{f_{cm}(t)}{f_{cm}(28)}} E_c(28) \quad (28)$$

in which

$$f_{cm}(t) = \frac{t_0}{\beta + \omega t_0} f_{cm}(28)$$

where

$f_{cm}(t)$ = time-dependent compressive strength of concrete

$f_{cm}(28)$ = compressive strength of concrete at 28 days

$E_c(28)$ = modulus of elasticity of concrete at 28 days

β = parameter that depends on the concrete mixture proportions and curing, which is taken as 4.0²⁹

ω = parameter that depends on the concrete mixture proportions and curing, which is taken as 0.85²⁹

The insulation was assumed to be nonaging linear viscoelastic and was modeled using the Maxwell chain model with ex-

pansion of the relaxation modulus into a Dirichlet series. The creep parameters were obtained from Gnip et al.,³² who proposed an exponential law for the creep strain $\varepsilon(t)$ as follows:

$$\varepsilon(t) = \varepsilon_0 + b_0 \left[1 - \exp(-b_1 t^{b_2}) \right]$$

where

ε_0 = initial strain

b_0 = parameter that was determined by experimental testing, taken as 5.705, for insulation with density of 20.7 kg/m³ (34.9 lb/yd³) that was tested under a sustained compressive stress σ_0 of 42.6 kPa (6.18 psi)

b_1 = parameter that was determined by experimental testing, taken as 0.0339, for insulation with density of 20.7 kg/m³ (34.9 lb/yd³) that was tested under a sustained compressive stress σ_0 of 42.6 kPa (6.18 psi)

b_2 = parameter that was determined by experimental testing, taken as 0.3103, for insulation with density of 20.7 kg/m³ (34.9 lb/yd³) that was tested under a sustained compressive stress σ_0 of 42.6 kPa (6.18 psi)

The relaxation modulus for the insulation was assumed to be equal to the effective modulus and taken as $\sigma_0/\varepsilon(t)$. Five Dirichlet terms were used.

The FRP reinforcing bars were considered linear elastic. Their potential creep response was neglected following Nkurunziza et al.³³ and Youssef and Benmokrane,³⁴ who reported that the creep strain is insignificant in GFRP bars. The steel reinforcement was also assumed linear elastic. The elastic modulus of the insulation layer that was made from EPS or XPS was taken as 5 or 10 MPa (0.73 or 1.45 ksi), respectively, based on data from the manufacturer.

Results and discussion

Nine concrete cylinders 100 mm (4 in.) in diameter and 200 mm (8 in.) in height were prepared to determine the tensile and compressive strength and the modulus of elasticity of concrete (three cylinders for each test). At the age of 28 days, the average elastic modulus of concrete was measured as 35.1 GPa (5090 ksi), the compressive strength was 63 MPa (9.1 ksi), and the tensile strength obtained from indirect (Brazil) testing was 4.4 MPa (0.64 ksi). The reinforcement used in the experiment had a Young's modulus of 206 GPa (29,900 ksi) and a yield stress of 585 MPa (84.8 ksi) based on the manufacturer's data. The ultimate strength and modulus of elasticity of the GFRP reinforcing bars were experimentally measured following ASTM-D7205/D7205M³⁵ as 800 MPa and 40 GPa (116 and 5800 ksi), respectively.

The strain measured in the prisms is the nominal shrinkage strain, which is usually considered for structural analysis and design in practice. During the first 14 days of drying, the shrinkage strain increased significantly and continued to increase at a lower rate between 14 and 21 days. At the age of 28 days, the measured average shrinkage strain in the standard shrinkage prisms was 505×10^{-6} . **Figure 5** shows the measured strain distributions through the thickness of the five panels with different geometric configurations. The strain development through the top layer of panel 1, which was not restrained, varied through the thickness because only the top surface was exposed to the environment and it underwent more drying shrinkage than the other points through the thickness of the layer. The measured strains at the top surface were slightly higher than the shrinkage strain measured in the prisms. This is attributed to size effects and to the nonuniform exposure conditions at the surfaces of the top layer of panel 1. The prisms were exposed to drying on all surfaces, while the top layer of panel 1 was only exposed to the environment at its top and side surfaces.

The results obtained from the bottom layer of panel 1 show that the steel reinforcement restrained shrinkage, leading to lower total strains, particularly near the exposed surface. The differences between the strains in the top and bottom concrete layers in panel 1 were a result of tensile stresses that developed in the concrete due to the restraint caused by the steel reinforcement. The top layer in panel 2 was similar to the bottom layer of panel 1 except that it was bonded to the EPS insulation. The bonding at the concrete-to-insulation interface slightly reduced the measured strains. Panels 2 and 3 had the same geometric configurations, but panel 3 used XPS insulation instead of EPS insulation. Slightly higher strains were developed in the midthickness of panel 3 compared with panel 2. This could be because XPS insulation has a smoother surface compared with EPS, which provides less restraint to the free shrinkage of concrete.

Panel 4 was similar to panel 2 except that it had continuous GFRP diagonal reinforcing bars as shear connectors. The results show that the addition of diagonal reinforcing bars seemed to significantly influence the strain distribution. The peak strains at the top surface for panel 4 were reduced by about 18% compared with panel 2 because of the addition of two lines of GFRP reinforcing bars. The differences in the strains resulted from the composite action that was provided by the shear connectors. Panels 4 and 5 had similar reinforcement ratios but different thicknesses and diameters of the GFRP reinforcing bars. The strain distributions in both panels 4 and 5 were found to be nearly uniform through the thickness. Overall, the strain distributions seemed to be more uniform when more restraints to the free shrinkage of concrete were added.

The five PCSPs tested in the laboratory were also analyzed by the FEA model. A bilinear shrinkage strain distribution was assumed through the thickness of the top concrete layer based on the data collected from panel 1 (Fig. 5). The same

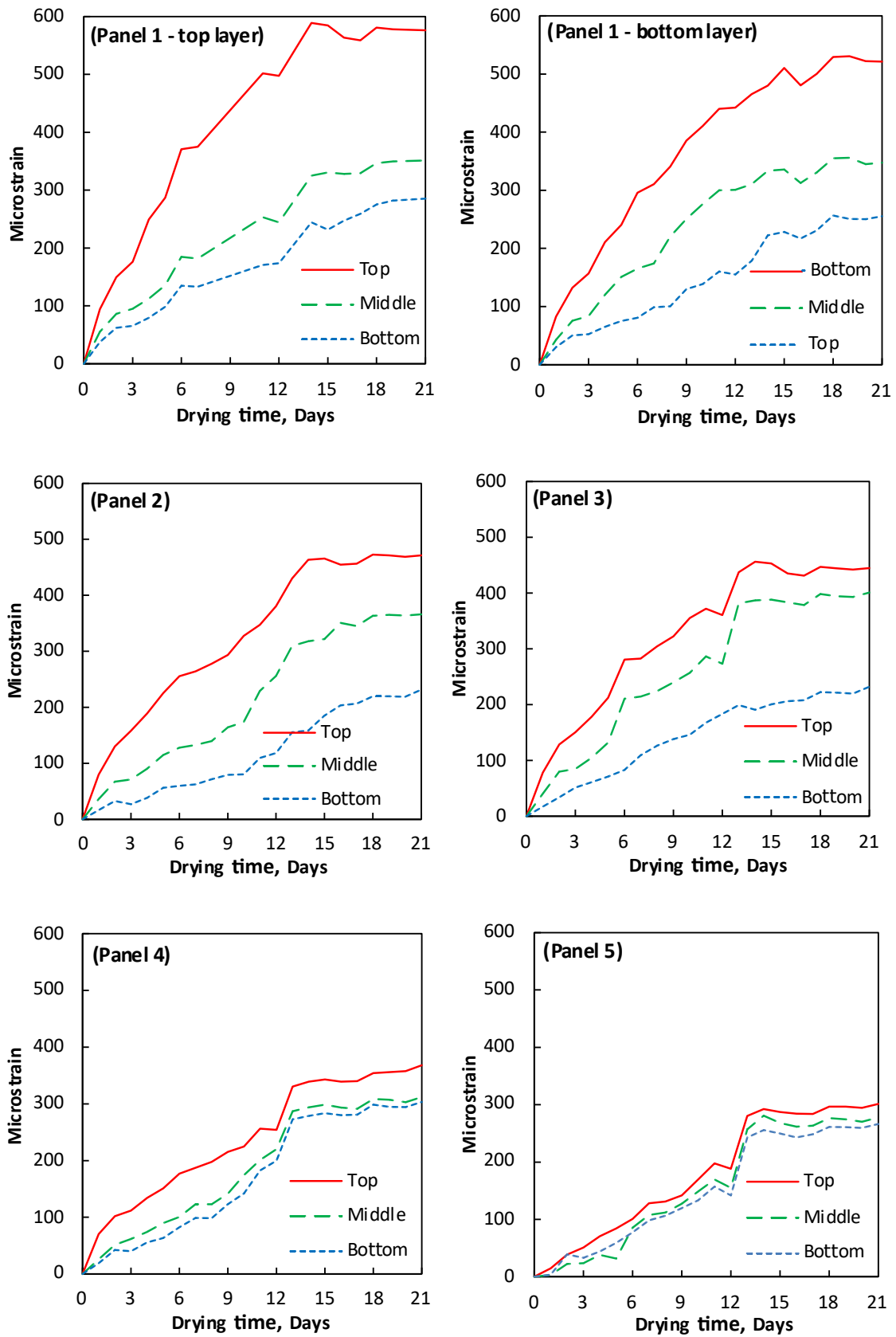


Figure 5. Measured strain development in panels 1 to 5.

shrinkage profile from the outer concrete surface to the concrete-to-insulation interface was assumed in the bottom concrete layer. The goal of the FEA was to apply a known bilinear shrinkage profile to the structure and compare the strains from the analysis with the strains measured in the tests. The shrinkage-induced strains and stresses predicted by the FEA model are shown in **Figures 6 and 7** through the thickness of the top layer, along with the measured strain profile in each panel. The results include the self-weight of the panels. Readings of the strains were taken only at midspan (a distance of 675 mm [26.6 in.] from both edges), and the averages are

shown in the figures. However, with the three-point supporting system (Fig. 3), the maximum stresses developed at the internal support. Therefore, the stresses at the internal support that were obtained from the FEA are also shown in Figures 6 and 7.

The predicted strain distributions correlated well with the measurements. The slight difference can be attributed to the creep and aging models used in the FEA, which may not exactly reflect the concrete properties in the tests. The predicted stresses in the PCSPs were relatively high. For example, the

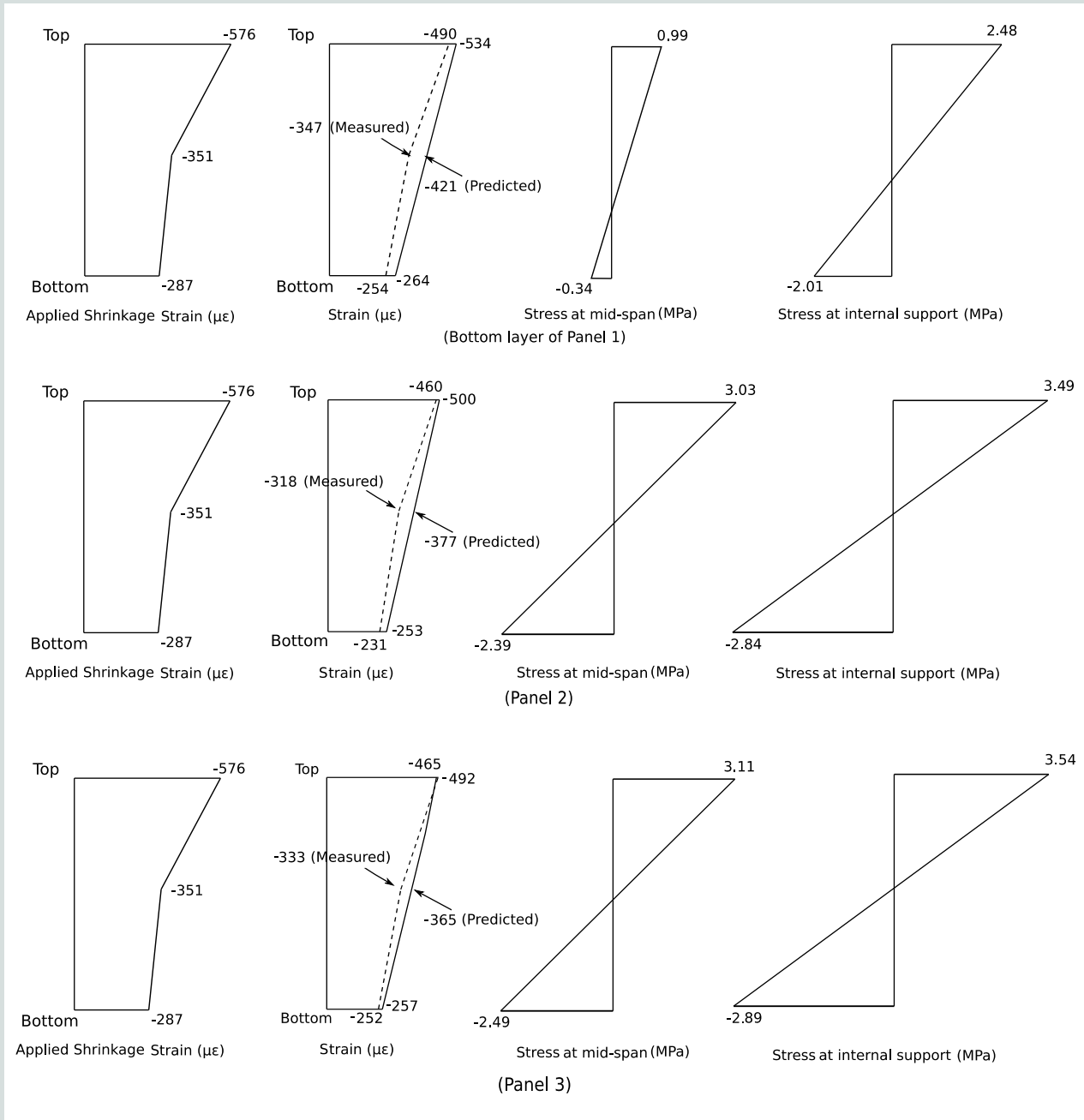


Figure 6. Predicted and measured strains and stresses in panels 1 to 3. Note: $\mu\epsilon$ = microstrain. 1 MPa = 0.145 ksi.

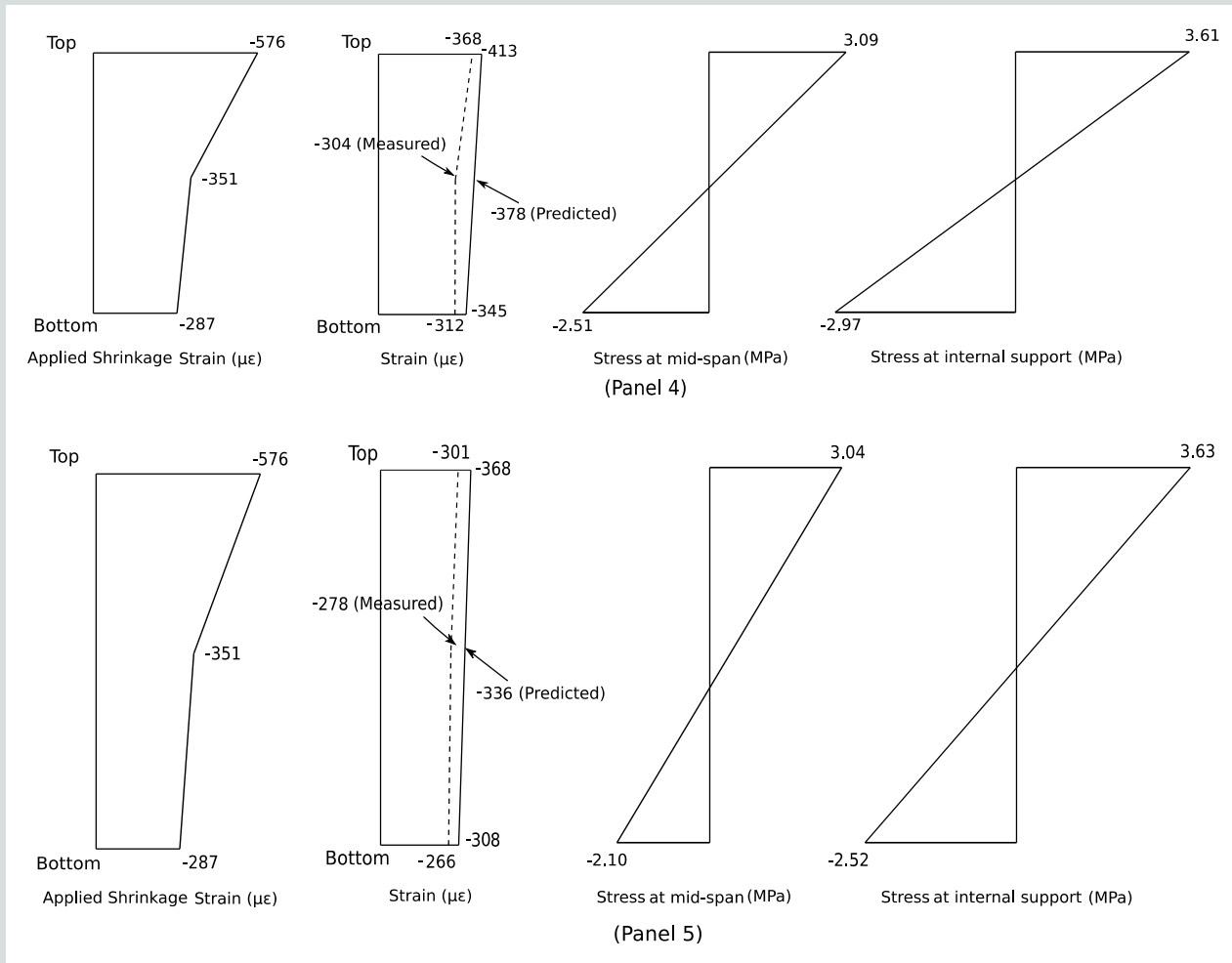


Figure 7. Predicted and measured strains and stresses in panels 4 and 5. Note: $\mu\epsilon$ = microstrain. 1 MPa = 0.145 ksi.

tensile stress at the top surface of panel 5 was about 80% of the uniaxial tensile strength of the concrete, which indicates a large reduction in the cracking moment caused by shrinkage effects. In different scenarios that include different types of concrete or when sufficient moist curing is not provided, shrinkage may lead to early-age cracking of PCSPs. Figures 6 and 7 also show that, as expected, when more restraint to shrinkage was provided, higher tensile stresses developed at the top surface.

The FEAs were based on the assumption of bilinear shrinkage strain distribution through the thickness of the concrete layer, with strain magnitudes based on the test measurements. However, in design practice, a uniform shrinkage strain distribution is commonly assumed through the thickness and a linear distribution is assumed in more advanced analyses. Panel 5 was reanalyzed under different shrinkage strain distributions to investigate and clarify the accuracy of the strain distribution assumptions (**Fig. 8**). The magnitude of the uniform shrinkage profile was taken from the measurement of the prisms. The linear shrinkage distribution was obtained from panel 1 in Figure 5 by taking the strains at the top and bottom surfaces. Figure 8

shows that the uniform strain distribution greatly overestimated the total strains. The linear shrinkage distribution also overestimated the strain, but it generated more accurate results than the uniform shrinkage profile. Therefore, a bilinear distribution of shrinkage provides more accurate and reliable results for predicting the early-age structural behavior of PCSPs.

Figure 9 shows the effect of changing the diameter of steel reinforcement on the maximum tensile stress of the top reinforced concrete layer. The diameter of the FRP bars was 6 mm (0.24 in.). The diameter of the steel reinforcement ranged from 6 to 12 mm (0.47 in.), which corresponds to a reinforcement ratio between 0.0038 and 0.016. As expected, increasing the diameter of steel reinforcement caused a higher restraint to shrinkage and increased the tensile stress in the concrete layer from 3.61 to 4.98 MPa (0.52 to 0.72 ksi). Because the tensile strength of the concrete was 4.4 MPa (0.64 ksi), a reinforcement ratio greater than 0.011 can cause cracking in the concrete layers in this case. Although they are not shown here, the effects of the diameter of the FRP diagonal bar were also investigated. The results revealed that it had very little influence on the shrinkage-induced tensile stress in concrete.

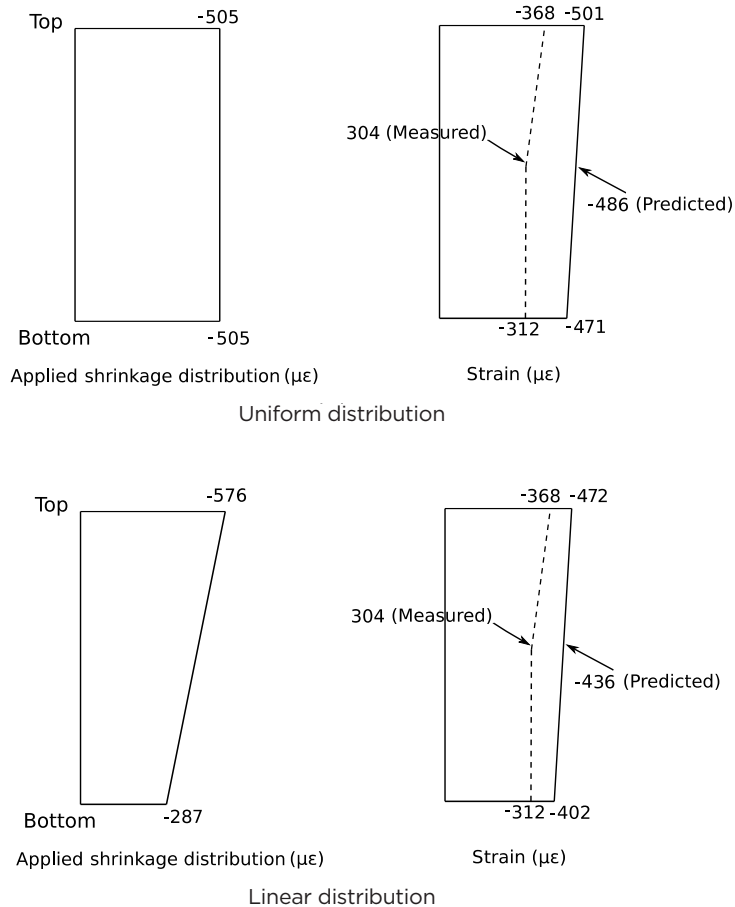


Figure 8. Predicted strains in panel 5 using different shrinkage distributions. Note: $\mu\epsilon$ = microstrain.

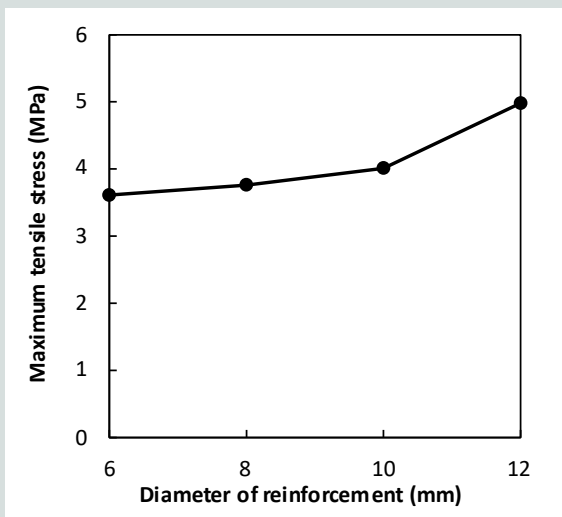


Figure 9. Influence of the diameter of steel reinforcement. Note: 1 mm = 0.03937 in.; 1 MPa = 0.145 ksi.

Conclusion

An experimental study and a numerical investigation were presented to investigate the effect of shrinkage on the early-age behavior of PCSPs. Early age refers to the first few weeks after casting while the panel is awaiting delivery to the construction site or has just been installed on the building. As such, no flexural loading at service is considered in this investigation. The results show that shrinkage-induced stresses were linear through the thickness of the concrete layers and changed from tension to compression, though the total strains were nearly uniform. Large tensile stresses that were about 80% of the tensile strength of concrete were developed. This indicates that cracking due to early-age shrinkage can happen in PCSPs if proper curing is not implemented or if the embedded reinforcement quantity, and the consequent restraint of shrinkage, is high. In cases where the concrete tensile strength is high enough to prevent early-age cracking, careful attention should be paid to the preexisting tensile stresses in the concrete. These stresses lead to a reduction in the cracking moment at serviceability, which can significantly influence the behavior under flexural loading.

The study shows that using a bilinear shrinkage profile through the thickness of each concrete layer in the analysis accurately predicts the early-age shrinkage effects, whereas the commonly used uniform shrinkage distribution can greatly overestimate the strains. The bilinear distribution was based on data collected from an unrestrained concrete layer with the same dimensions as the tested PCSPs. The peak value of the bilinear distribution at the exposed concrete surface was slightly larger than the value measured from standard shrinkage prisms, while the minimum value at the concrete-to-insulation interface was about half the strain measured from the prism test. Both the experimental and numerical results showed that the total strain distribution tends to be more uniform when more restraints are added into the panel. The magnitude of the uniform strains was about 60% of those obtained from standard shrinkage prisms.

The amount of steel reinforcement had a significant influence on the shrinkage-induced tensile stresses, whereas the diameter of the diagonal FRP reinforcing bars in the shear connectors had a minor influence. This is because the truss mechanism that evolves when diagonal-bar shear connectors are used is effective mainly under bending action and not under interfacial shear produced by the shrinkage action.

Acknowledgments

The work reported in this paper has been undertaken with the financial support of the Australian Research Council (ARC) through a Discovery Project (DP160102027). The support is greatly acknowledged. The authors would also like to thank Graeme McGregor and OneSteel Reinforcing for supplying the steel reinforcement for the experimental work.

References

1. PCI Industry Handbook Committee. 2010. *PCI Design Handbook: Precast and Prestressed Concrete*. MNL-120. 7th ed. Chicago, IL: PCI.
2. PCI Architectural Precast Concrete Services Committee. 2007. *Architectural Precast Concrete*. 3rd ed. MNL-122. Chicago, IL: PCI.
3. NPCAA (National Precast Concrete Association Australia). 2012. *Recommended Practice: Precast Concrete Sandwich Panels*. Glenelg, Australia: NPCAA.
4. Einea, A., D. C. Salmon, M. K. Tadros, and T. Culp. 1994. "A New Structurally and Thermally Efficient Precast Sandwich Panel System." *PCI Journal* 39 (4): 90–101.
5. PCI Committee on Precast Sandwich Wall Panels. 2011. "State of the Art of Precast/Prestressed Concrete Sandwich Wall Panels, Second Edition." *PCI Journal* 56 (2): 131–176.
6. Gilbert, R. I. 1988. *Time Effects in Concrete Structures*. Amsterdam, Netherlands: Elsevier.
7. Gilbert, R. I., and G. Ranzi. 2010. *Time-Dependent Behaviour of Concrete Structures*. New York, NY: CRC Press.
8. Bažant, Z. P., and F. H. Wittmann. 1982. *Creep and Shrinkage in Concrete Structures*. New York, NY: John Wiley and Sons.
9. NPCAA. 2013. *Curing Wet-Cast Precast Concrete*. Glenelg, Australia: NPCAA.
10. Salmon, D. C., M. K. Tadros, and T. Culp. 1994. "A New Structurally and Thermally Efficient Precast Sandwich Panel System." *PCI Journal* 39 (4): 90–101.
11. Salmon, D. C., and A. Einea. 1995. "Partially Composite Sandwich Panel Deflections." *Journal of Structural Engineering* 121 (4): 778–783.
12. Pigeon, M., G. Toma, A. Delagrave, B. Bissonnette, J. Marchand, and J. C. Prince. 2000. "Equipment for the Analysis of the Behaviour of Concrete under Restrained Shrinkage at Early Ages." *Magazine of Concrete Research* 52 (4): 297–302.
13. Weiss, W. J., W. Yang, and S. P. Shah. 1998. "Shrinkage Cracking of Restrained Concrete Slabs." *Journal of Engineering Mechanics* 124 (7): 765–774.
14. Kovler, K. 1994. "Testing System for Determining the Mechanical Behaviour of Early Age Concrete under Restrained and Free Uniaxial Shrinkage." *Materials and Structures* 27 (6): 324–330.
15. Sule, M., and K. van Breugel. 2001. "Cracking Behaviour of Reinforced Concrete Subjected to Early-Age Shrinkage." *Materials and Structures* 34 (5): 284–292.
16. Altoubat, S. A., and D. A. Lange. 2001. "Creep, Shrinkage and Cracking of Restrained Concrete at Early Age." *ACI Materials Journal* 98 (4): 323–331.
17. Khan, I., A. Murray, A. Castel, and R. I. Gilbert. 2015. "Experimental and Analytical Study of Creep and Shrinkage in Early-Age Concrete." In *CONCREEP 10: Mechanics and Physics of Creep, Shrinkage, and Durability of Concrete and Concrete Structures*, ed. C. Hellmich, B. Pichler, and J. Kollegger. <https://doi.org/10.1061/9780784479346.128>.
18. Gilbert, R. I. 2017. "Cracking Caused by Early-Age Deformation of Concrete—Prediction and Control." *Procedia Engineering* 172: 13–22.
19. Gilbert, R. I., M. A. Bradford, A. Gholamhoseini, and Z. T. Chang. 2012. "Effects of Shrinkage on the Long-

Term Stresses and Deformations of Composite Concrete Slabs.” *Engineering Structures* 40: 9–19.

20. Gholamhoseini, A., R. I. Gilbert, M. Bradford, and Z. T. Chang. 2014. “Time-Dependent Deflection of Composite Concrete Slabs.” *ACI Structural Journal* 111 (4): 765–776.
21. Al-deen, S., and G. Ranzi. 2015. “Effects of Non-uniform Shrinkage on the Long-Term Behaviour of Composite Steel-Concrete Slabs.” *International Journal of Steel Structures* 15 (2): 415–432.
22. Kim, J. K., and C. S. Lee. 1998. “Prediction of Differential Drying Shrinkage in Concrete.” *Cement and Concrete Research* 28 (7): 985–994.
23. Bažant, Z. P., and L. J. Najjar. 1972. “Nonlinear Water Diffusion in Non-saturated Concrete.” *Materials and Structures* 5 (1): 3–20.
24. Bažant, Z. P., and W. Thonguthai. 1978. “Pore Pressure and Drying of Concrete at High Temperature.” *Journal of Engineering Mechanics* 104 (5): 1059–1079.
25. Illston, J. M., and A. Tajirian. 1977. “Computer Experiments on Environmentally Induced Stresses in Unreinforced Concrete Pavement Slabs.” *Magazine of Concrete Research* 29 (101): 175–190.
26. Sakata, K. 1983. “A Study on Moisture Diffusion in Drying and Drying Shrinkage of Concrete.” *Cement and Concrete Research* 13 (2): 216–224.
27. Huang, Q., and E. Hamed. 2019. “Nonlinear Finite Element Analysis of Composite Precast Concrete Sandwich Panels Made with Diagonal FRP Bar Connectors.” *Composite Structures* 212: 304–316.
28. Bažant, Z. P., and S. T. Wu. 1974. “Rate-Type Creep Law of Aging Concrete Based on Maxwell Chain.” *Matériaux et Construction* 7 (1): 45–60.
29. ACI (American Concrete Institute) Committee 209. 2008. *Prediction of Creep, Shrinkage, and Temperature Effects in Concrete Structures*. ACI 209R-92. Farmington Hills, MI: ACI.
30. Carol, I., and Z. P. Bažant. 1993. “Viscoelasticity with Aging Caused by Solidification of Nonaging Constituent.” *Journal of Engineering Mechanics* 119 (11): 2252–2269.
31. Bažant, Z. P., and S. Prasannan. 1989. “Solidification Theory for Concrete Creep.” *Journal of Engineering Mechanics* 115 (8): 1691–1725.
32. Gnip, I. Y., S. Vaitkus, V. Keršulis, and S. Vjelij. 2011. “Analytical Description of the Creep of Expanded Poly-

styrene (EPS) under Long-Term Compressive Loading.” *Polymer Testing* 30 (5): 493–500.

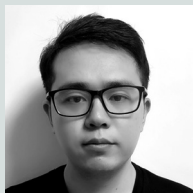
33. Nkurunziza, G., B. Benmokrane, A. S. Debaiky, and R. Masmoudi. 2005. “Effect of Sustained Load and Environment on Long-Term Tensile Properties of Glass Fiber-Reinforced Polymer Reinforcing Bars.” *ACI Structural Journal* 102 (4): 615–621.
34. Youssef, T., and B. Benmokrane. 2011. *Creep Behavior and Tensile Properties of GFRP Bars Under Sustained Service Loads*. Special Publication 275. Farmington Hills, MI: ACI.
35. ASTM Subcommittee D30.10. 2016. *Standard Test Method for Tensile Properties of Fiber Reinforced Polymer Matrix Composite Bars*. ASTM-D7205/D7205M. West Conshohocken, PA: ASTM International.

Notation

- | | |
|--------------|---|
| b_0 | = parameter that was determined by experimental testing, taken as 5.705, for insulation with density of 20.7 kg/m ³ (34.9 lb/yd ³) that was tested under a sustained compressive stress σ_0 of 42.6 kPa (6.18 psi) |
| b_1 | = parameter that was determined by experimental testing, taken as 0.0339, for insulation with density of 20.7 kg/m ³ (34.9 lb/yd ³) that was tested under a sustained compressive stress σ_0 of 42.6 kPa (6.18 psi) |
| b_2 | = parameter that was determined by experimental testing, taken as 0.3103, for insulation with density of 20.7 kg/m ³ (34.9 lb/yd ³) that was tested under a sustained compressive stress σ_0 of 42.6 kPa (6.18 psi) |
| d | = constant for determining the creep coefficient |
| E_c | = modulus of elasticity of concrete |
| $E_c(t)$ | = time-dependent modulus of elasticity of concrete |
| $E_c(28)$ | = modulus of elasticity of concrete at 28 days |
| E_μ | = modulus of the μ th spring in the Maxwell chain |
| $E_\mu(t)$ | = modulus of the μ th spring in the Maxwell chain for a strain applied at time t |
| $E_\mu(t')$ | = modulus of the μ th spring in the Maxwell chain for a strain applied at time t' |
| $f_{cm}(t)$ | = compressive strength of concrete at time t |
| $f_{cm}(28)$ | = compressive strength of concrete at 28 days |

- n = number of spring-dashpot units
- $R(t,t')$ = relaxation modulus of concrete
- $R'(t,t')$ = approximated relaxation modulus of concrete
- t = time
- t' = time of applied load
- t_0 = time of initial loading
- β = parameter that depends on the concrete mixture proportions
- γ_c = cumulative product of correction factors
- ε_0 = initial strain
- $\varepsilon(t)$ = creep strain
- $\zeta(t)$ = aging function
- μ = unit number
- σ_0 = sustained stress
- τ_μ = relaxation time of the μ th unit
- ϕ = creep coefficient
- ϕ_u = final creep coefficient
- $\phi(t,t')$ = creep coefficient of concrete at time t for a load applied at t'
- ψ = constant for determining the creep coefficient
- ω = parameter that depends on the concrete mixture proportions

About the authors



Qian Huang, is a PhD student in the School of Civil and Environmental Engineering at the University of New South Wales (UNSW) in Kensington, Australia. His thesis deals with the time-dependent behavior of precast concrete sandwich panels.



Ehab Hamed, PhD, is an associate professor in the School of Civil and Environmental Engineering at UNSW and a member of its Centre for Infrastructure Engineering and Safety. He received his PhD in 2007 from the Technion–Israel Institute of Technology.

His research interests include modeling and analysis of concrete structures, creep and shrinkage of concrete, sandwich panels, and the retrofitting of steel and concrete structures with composite materials.



Ian Gilbert, PhD, is emeritus professor at UNSW within the UNSW Centre for Infrastructure Engineering and Safety. His research interests are in the area of serviceability and the time-dependent behavior of reinforced and prestressed concrete structures. He

has published eight books and more than 350 papers in refereed journals and conferences. He is a member of Standards Australia's Concrete Structures code committee, and he has been actively involved in the development of the Australian Standard AS 3600 for more than 35 years.

Abstract

An experimental study that investigates the shrinkage effects at early ages of five precast concrete sandwich panels with various configurations is presented. Wire strain gauges were embedded within the concrete panels to determine the strain profile in unloaded specimens. The results indicate that the steel reinforcement, the insulation, and the shear connectors in the panels all impose different degrees of restraint to shrinkage of concrete and these parameters can change the shrinkage-induced strains significantly. A two-dimensional finite element analysis (FEA) model that was verified by the experimental results was used to explain aspects of the structural behavior that could not be measured in the tests. The FEA model accounted for creep, shrinkage, and aging of concrete, as well as creep in the insulation, and it used a bilinear shrinkage profile within the thickness of the concrete layers. A parametric study was conducted to investigate key parameters in the design of precast concrete sandwich panels, including the profile of the shrinkage strain, total reinforcement ratio, and diameter of the diagonal-bar shear connectors.

Keywords

Concrete sandwich panel, cracking, creep, fiber-reinforced polymer, FRP, restraint, sandwich panel, shear connector, shrinkage.

Review policy

This paper was reviewed in accordance with the Precast/Prestressed Concrete Institute's peer-review process.

Reader comments

Please address any reader comments to *PCI Journal* editor-in-chief Tom Klemens at tklemens@pci.org or Precast/Prestressed Concrete Institute, c/o *PCI Journal*, 200 W. Adams St., Suite 2100, Chicago, IL 60606. [f](#)